Astron. Astrophys. 328, 381–389 (1997)

ASTRONOMY AND ASTROPHYSICS

First observations with a new imaging polarimeter

A.M. Gandorfer and H.P. Povel

Institut für Astronomie, ETH-Zentrum, CH-8092 Zürich, Switzerland

Received 29 April 1997 / Accepted 15 July 1997

Abstract. We present first observations of solar polarization with a new imaging polarimetry system that simultaneously records three Stokes components, I, Q, V or I, U, V, in a single CCD. This instrument is an intermediate version on the way to ZIMPOL II (Zürich Imaging Stokes Polarimeter II), which will record all four Stokes parameters (Stenflo et al. 1992). The principle of operation is based on a piezoelastic polarization modulator in combination with a special CCD sensor equipped with a microlens array and a mask. This sensor is used as a synchronous demodulator. The theoretical performance of the instrument is discussed. Laboratory tests as well as initial solar observations at two different solar telescopes are presented and analysed to experimentally evaluate the performance. The polarimetric accuracy is better than 10^{-4}, a noise level of 2×10^{-5} has been achieved; the polarimetric efficiency is in agreement with theory.

Key words: instrumentation: polarimeters – Sun: magnetic fields – polarization

1. Introduction

Many phenomena in the solar atmosphere have their origin in magnetic fields. Magnetism is responsible for the structural richness of the solar atmosphere, for solar activity, and it is also thought to play an important role in chromospheric and coronal heating. Solar magnetic fields are best observed in polarized light. Light becomes polarized in the presence of magnetic fields via the Zeeman effect, and light, polarized by resonant scattering near the solar limb can be partly depolarized in the presence of magnetic fields via the Hanle effect (Stenflo 1982, Stenflo 1994). To investigate solar magnetic fields efficiently, one requires sequences of "polarization images", each consisting of linear combinations of two or more photometric or spectral images taken in different polarization states. Such measurements are disturbed by three main noise sources:
1. Atmospheric seeing in the form of blurring and image motions on time scales of typically 10 ms.
2. Gain table or flatfield noise. This arises when the two images that represent orthogonal polarization states fall on different detecting areas, as done in beam splitter systems. Photocharges are generated by elements with differing photosensitivity.
3. Photon noise.
While the last noise source can be suppressed only by increasing the integration time, the other two can be avoided by instrumental concepts. In the ZIMPOL I system (Povel et al. 1990; Keller et al. 1992; Stenflo 1994; Povel et al. 1994; Povel 1995) seeing noise is eliminated by fast polarization modulation in the tens of kHz range, and gain table effects are avoided by using the same pixels for each differential polarization measurement. Since the read-out frequency of a CCD is far too low to read out the frames in synchronism with the fast modulation, one creates two image planes in the CCD sensor by masking every second row with an opaque mask. Charge packages created in an unmasked row during one half period of the modulation are shifted to the next masked row, which is used for temporary buffer storage, in synchronism with the fast modulation. In this way two interlaced images are created in the same CCD (a similar principle was first suggested by Stockman (1982) for differential imaging in astronomical applications. In that work, the 512 $\times$ 320 CCD sensor area was divided into three sections of equal size, two for charge storage and one that was photosensitive. Each section extended over 170 rows. However, only slow modulation frequencies from 0.1 to 1 Hz were tested.).

After many thousands of modulation periods the sensor is read out. The sum of the two images is proportional to the intensity, their normalized difference is proportional to one Stokes component of the degree of polarization. The fractional polarization is formed by taking differences between the two images and dividing them by the sum image. The gain table scaling factors, which are identical for both images then simply divide out. The differential measurements are obtained nearly simultaneously as compared with the seeing time scale. In this way no mixture of polarization is induced apart from smearing of the image. To measure the complete Stokes vector (I, Q, U, V) (two linear polarizations and circular polarization) one uses two piezoelastic modulators at two different frequencies and three CCD cameras, each detecting one polarized Stokes parameter. The ZIMPOL I system has been used with great succes in recent years (Keller et al. 1994, Rüedi et al. 1996, Bernasconi et

Send offprint requests to: A. Gandorfer

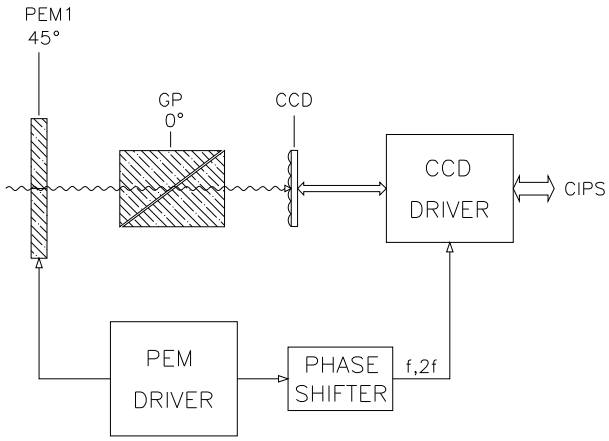

Fig. 1. Block diagram of the polarimeter. The polarization is modulated by a piezoelastic modulator (PEM1) followed by a Glan linear polarizer (GP). The CCD driver is connected to a control and image processing system (CIPS).

al. 1997). The noise level is 10^{-3} in a single exposure and can be reduced to 5×10^{-6} by frame averaging (Stenflo and Keller 1996).

There are, however, three disadvantages to the above system: 1) A factor of three in intensity is lost by using three cameras. 2) Another factor of two is lost by the mask, which blocks every other pixel row. 3) The use of three cameras has the additional disadvantage that the three images have to be matched (involving image rotation and pixel extrapolation) to combine them to form Stokes vector images.

These disadvantages can be eliminated if one uses only one camera to detect all three normalized Stokes parameters; this is the concept of ZIMPOL II (Stenflo et al. 1992). By masking three out of four rows of the CCD, one can create four interlaced charge images in one CCD, corresponding to four optical images, each for a different phase interval of the modulation. A phase-locked double modulator then allows simultaneous recording of the full Stokes vector. To optimize the signal and not lose photons by masking $3/4$ of the detecting surface, the chip is covered with an array of cylindrical microlenses, which have the same width as four pixel rows and focus the photons into the unmasked row. However, a phase-locked dual piezoelastic modulator has not yet been realized. As an intermediate step, a polarimeter system consisting of the new CCD sensor with only one piezoelastic modulator has been built, which allows for the first time the simultaneous detection of three Stokes vector components, I,Q,V or I,U,V in a single CCD.

2. Description of the instrument and its performance

For simultaneous measurement of circular and one linear polarization, the polarimeter consists of a piezoelastic modulator followed by a Glan polarizer and the special CCD chip with a replicated microlens-mask assembly (see Fig. 1).

The concept of detecting polarized light by modulation and synchronous demodulation consists in converting the polarization information into a time-dependent intensity information $I(t)$ by changing the transmission of the optical system periodically for the different polarization states. $I(t)$ is the sum of characteristic modulated intensity functions $I_j(t)$ for the Stokes parameters $j = I, Q, U, V$. These intensity functions will be called *modulation functions*. Each Stokes parameter corresponds to a modulation function of characteristic frequency and phase. By dividing the modulation period into four sampling intervals of equal length and integrating the signal $I(t)$ during these four intervals, one obtains four signals. It is possible to find linear combinations of them to extract the polarization information. The modulator package can be represented by its Mueller matrix (e.g. Collet 1993)

$$\mathbf{M} = \frac{1}{2}\begin{pmatrix} 1 & \cos\delta & 0 & -\sin\delta \\ 1 & \cos\delta & 0 & -\sin\delta \\ 0 & 0 & 0 & 0 \\ 0 & 0 & 0 & 0 \end{pmatrix}.$$

A piezoelastic modulator has a time-dependent retardation $\delta(t)$. In a fused silica slab, which is optically isotropic under normal conditions, a standing acoustic wave is generated by exciting the slab with a piezoelectrical transducer at its mechanical resonance frequency. The mechanical stress produces optical anisotropy and thus birefringence. The optical retardation depends on the oscillation amplitude. As the mechanical vibration is sinusoidal, the retardation is given by

$$\delta(t) = A \sin \omega t,$$

where A is the amplitude retardation and ω is 2π times the modulation frequency. For more information about piezoelastic modulators, see Kemp (1969). Inserting $\delta(t)$ in $\mathbf{M}$ gives

$$\mathbf{M} = \frac{1}{2}\begin{pmatrix} 1 & \cos(A\sin\omega t) & 0 & -\sin(A\sin\omega t) \\ 1 & \cos(A\sin\omega t) & 0 & -\sin(A\sin\omega t) \\ 0 & 0 & 0 & 0 \\ 0 & 0 & 0 & 0 \end{pmatrix}.$$

The Stokes vector $\boldsymbol{I}'$ of the transmitted light is given by the product $\mathbf{M}\boldsymbol{I}$. The first component of $\boldsymbol{I}'$ is the modulated intensity

$$I(t) = \frac{1}{2}(I + \cos(A\sin\omega t)Q - \sin(A\sin\omega t)V).$$

From the expansion of the trigonometric expressions in terms of Bessel functions (see also Sect. 3) it follows that Q is modulated with 2ω (and all even higher harmonics), while V is modulated at ω (and all odd higher harmonics). For the two special cases of purely linearly and purely circularly polarized light, the resulting modulation functions are plotted in Fig. 2.

All polarization information is encoded in the modulation function. In the four interlaced image planes of the ZIMPOL II CCD sensor four charge packages are accumulated during four sampling intervals in phase with the fast modulation. This is achieved by shifting the four charge packages to and fro in the masked CCD chip, in such a way, that only one package is accessible to photons during a sampling interval. In this way, each

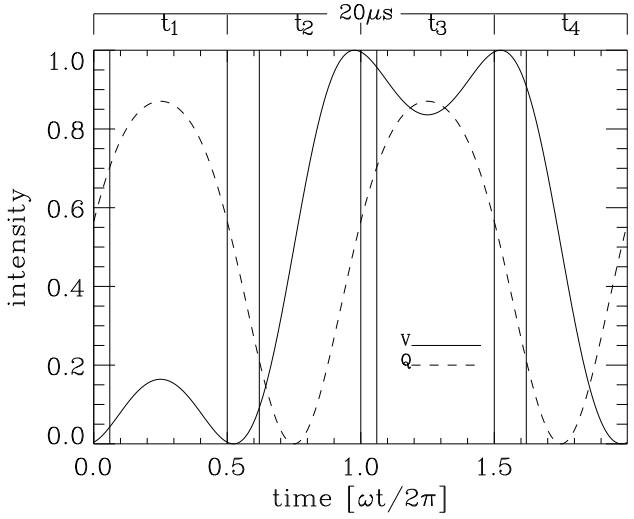

Fig. 2. Modulation functions for 100% linearly (Q) or circularly (V) polarized light. Stokes Q is modulated at 2ω, while Stokes V is modulated at ω. At the beginning of each demodulation time interval $t_{1,2,3,4}$ the charge packages are shifted by one pixel (0.6μs) or two pixels (1.2μs), according to the shifting scheme (see text).

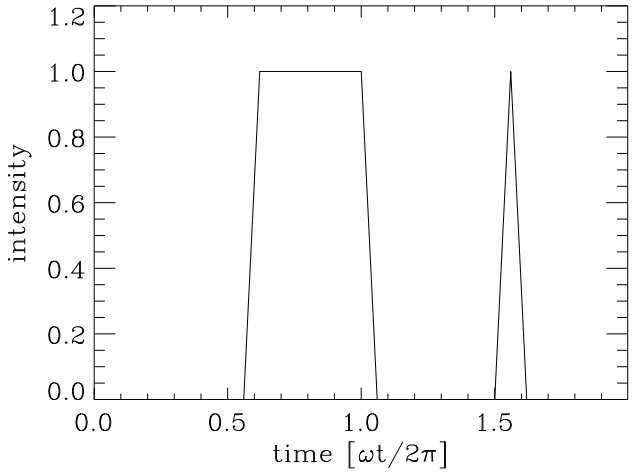

Fig. 3. Intensity of unmodulated light seen by the charge package q_3 during one demodulation cycle (the "window function").

charge package reflects the integral of the modulation function during a quarter of the period of modulation. The polarization information is decoded after readout of the integrated charge packages by forming linear combinations of these charge packages.

The great advantage of the ZIMPOL II principle is that all four image planes are generated by the same set of physical pixels. The different image planes are illuminated by sequentially shifting the charges between the pixel rows, but it is always the same photosensitive elements that are illuminated in all four image planes. The gain tables of the four image planes are therefore identical, which means that the fractional polarization images $Q/I, U/I$, and V/I are free from gain-table or flat-field effects.

However, the photo charges cannot be shifted instantaneoulsy. Due to the electrical properties of the CCD, the charge transfer time has a lower limit. In the EEV CCD 002-06 chip used here the time needed to shift a charge package from one row to the next is 600 ns. This has an influence on the accumulation of charge during the sampling process. To make this perturbing effect as symmetric as possible for the four samplings, the shifting sequence is: During t_1 charge package q_1 is exposed. After a double shift q_3 is exposed during t_2. q_4 is exposed during t_3, and - after a double shift - q_2 is exposed during t_4:

$$t_1 \longrightarrow t_2 \longrightarrow t_3 \longrightarrow t_4 \longrightarrow t_1.$$

$$q_1 \longrightarrow q_3 \longrightarrow q_4 \longrightarrow q_2 \longrightarrow q_1.$$

Each charge package q_m ($m = 1, 2, 3, 4$) 'sees' light when it is shifted in or through the unmasked row, resulting in a characteristic aperture or 'window' function $a_m(\omega t)$. These window functions are plotted together with the modulation functions in Fig. 2. An example of the theoretical window function for the charge package q_3 is shown in Fig. 3.

The principle of demodulation is shown in Fig. 4. The accumulated charge is proportional to the integral of $a_m(\omega t)$ times the modulation function $I(t)$. While the sum of all four charge packages is proportional to the intensity, the ratio

$$C_{\rm lin} = (q_1 + q_4 - q_3 - q_2)/(q_1 + q_2 + q_3 + q_4)$$

is proportional to Stokes Q/I, and the ratio

$$C_{\rm circ} = (q_4 - q_1)/(q_1 + q_2 + q_3 + q_4)$$

is proportional to Stokes V/I. These values are maximum for purely polarized light. With a demodulation period of 20μs (corresponding to $\frac{\omega}{2\pi}$ =50 kHz) and 0.6μs charge transfer time, $C_{\rm lin,max}$=0.547 and $C_{\rm circ}$=0 for pure Stokes Q, while $C_{\rm circ,max}$=0.406 and $C_{\rm lin}$=0 for pure Stokes V. As in all modulation-demodulation techniques (lock-in, Boxcar) the measured signal depends on the phase angle between the modulation and demodulation cycles. This dependence was calculated and then measured in the laboratory by inserting a linear or a circular polarizer in the optical path in front of the modulator and manipulating the phase shifter. The measured and calculated curves are presented in Fig. 5 for a retardation amplitude of A = 2.4 radians (first zero of Bessel function, see also Sect. 3). The measured values agree well with the expected curve. The small discrepancy can be explained by a non perfect setting of the angle between the modulator and the polarizer ($\neq 45^\circ$) and by a small deviation of the modulation amplitude from its ideal value of 2.405.

2.1. System components

The EEV CCD02-06 three-phase buried-channel CCD sensor is used in frame transfer mode with 385 pixels per row and 288 pixels per column in the image and storage zones, respectively. The pixel size is 22μm $\times$22μm. The cylindrical microlenses are aligned parallel to the pixel rows and cover four rows each,

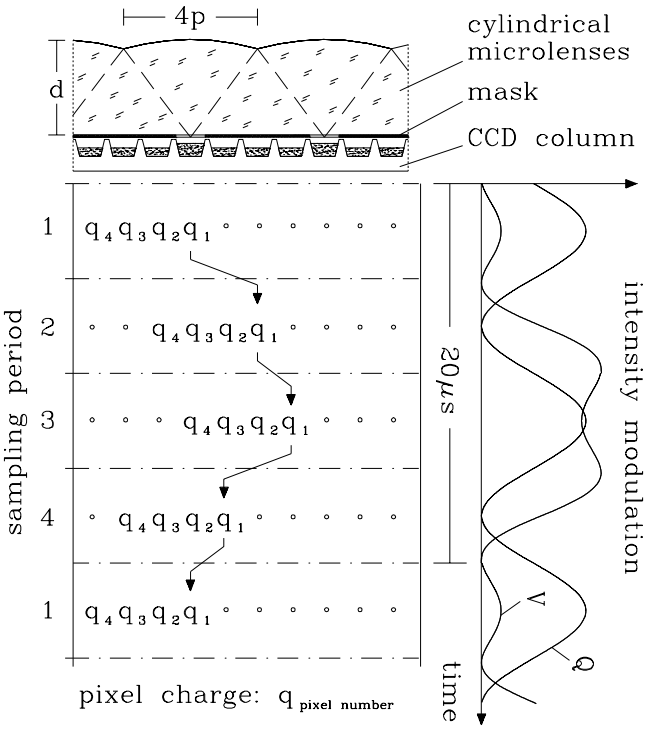

Fig. 4. Principle of the demodulation scheme. Upper part: Cross section of the microlens array in a plane perpendicular to the pixel rows. The vertical scale is compressed. 4p is typically 80 μm (p is the pixel size), d is on the order of 1 mm. Right part: Intensity modulation for Stokes Q and V. The modulation period is 20 μs (corresponding to 50 kHz). Central part: Position of the charge packages during the four sampling periods.

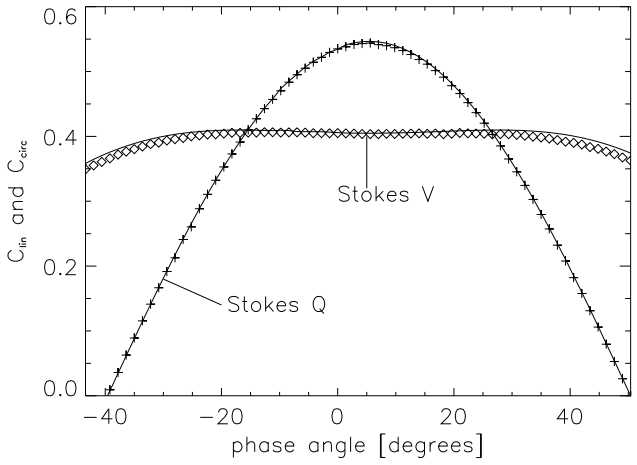

Fig. 5. Calculated (solid lines) and measured (crosses and diamonds) phase angle dependences of $C_{\rm lin,max}$ (pure Stokes Q) and $C_{\rm circ,max}$ (pure Stokes V). By adjusting the phase offset the measured curves have been shifted in the horizontal direction for optimum agreement with the theoretical curves.

one uncovered and three masked with a chromium layer, which is deposited on the back side of a 1 mm B 270 glass substrate carrying the replicated microlens array. For more information on the fabrication, mounting, and specifications of the microlens-mask-assembly, see Gale et al. (1996).

The modulator package consists of a PEM-80 piezoelastic modulator made by Hinds Instruments, Inc., U.S.A. The resonance frequency is 50 kHz. The modulator is followed by a Glan linear polarizer. For 50 kHz modulation frequency the charge shifting time of the CCD is 0.6 μs.

2.1.1. Tests of the microlens-array

A detailed description of the microlens tests can be found in Gale et al. (1996). The most important results are:

- The parasitic stray-light contributions in the masked rows adjacent to the unmasked row were measured to be less than 1% of the signal in the unmasked row. The stray-light distribution could be explained in terms of a simple model of the CCD surface: Photons are assumed not to be scattered in the microlenses but at the electrode structure of the CCD. With this model the lateral displacement and the rotation angle of the microlens-mask assembly could be determined from the measurements. The misalignment of the combined array relative to the CCD imager was estimated to be smaller than 0.7 μm in lateral position while the rotation is smaller than 0.005^o.
- The stray light varies over the CCD chip due to the rotation of the microlens-mask assembly with respect to the CCD. The resulting asymmetries turned out to be rather critical for the use of the polarimeter in high precision polarimetry. With detailed knowledge obtained from the test measurements, it was possible to find a calibration procedure (see Sect. 3) that takes the stray-light contributions properly into account.

2.1.2. Tests of the demodulator

The demodulation quality of the system was tested by inserting linear and circular polarizers in the optical path in front of the modulator package and comparing the measured signal with the expected one. The measured signals refer to each 'pixel quadruplet' (set of four neighboured pixels within one column used for demodulation), independent of gain-table or flat-field. All physical properties that are specific for each pixel (e.g. quantum efficiency) simply divide out and are therefore not critical. There is, however, a class of effects that is not connected to individual pixels, but varies from one pixel-quadruplet to the other: (1) Some pixels within a quadruplet have anomalously low and asymmetric charge transfer efficiencies and act as *charge traps*. (2) The scattering coefficients have different values for each quadruplet. These effects lead to a variation of the ratios $C_{\rm lin,max}$ and $C_{\rm circ,max}$ of the individual quadruplets over the detector surface. The array which presents these values for all pixel quadrupels is called the *polarization gain table*. It is measured by inserting polarization filters in front of the modulator package to produce 100 % Stokes Q and V. These *efficiency measurements* are performed under exactly the same conditions as the real measurements, i.e. with the same retardation, the same illumination geometry,

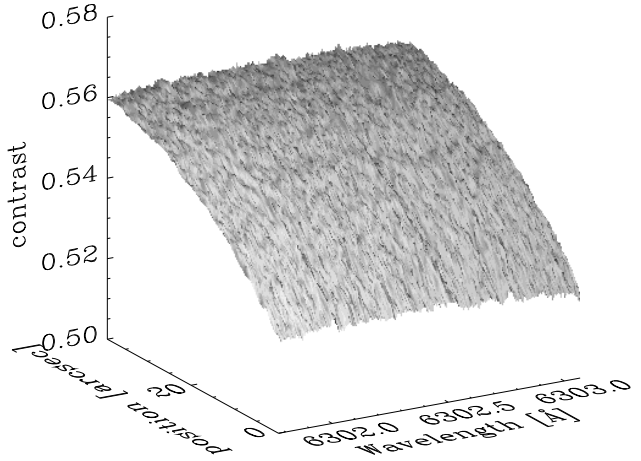

Fig. 6. Polarization gain table for Stokes Q/I, representing the Stokes Q/I calibration for the spectropolarimetric measurements in Fig. 9. The variation along the spatial direction arises from the sinusoidal mechanical stress distribution in the modulator (see Kemp 1969) that was placed before the entrance slit of the spectrograph.

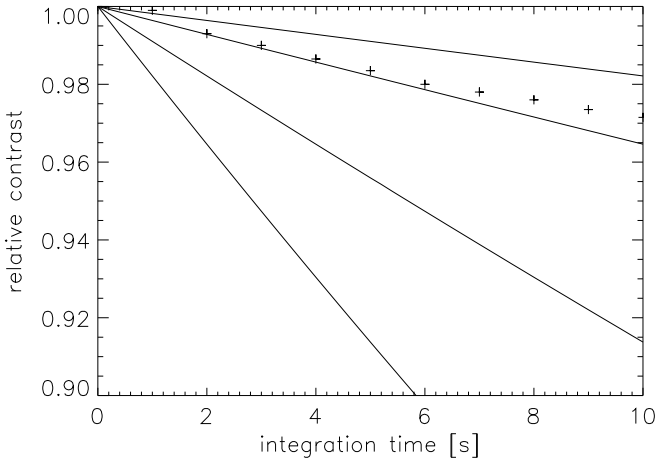

Fig. 7. Degradation of the linear polarization signal with integration time. 10 s of integration time corresponds to 5×10^5 shifting cycles. The crosses indicate measured values. The curves have been calculated for different charge transfer inefficiencies ϵ as explained in the text. ϵ varies from 10^{-8} (upper curve), to 2×10^{-8}, 5×10^{-8}, and 10^{-7} (lower curve).

and the same integration time. The last point is of special importance, because the observed ratio decreases with integration time due to charge transfer inefficiency.

An example of a polarization gain table is presented in Fig. 6. It represents the Stokes Q calibration for the spectropolarimetric measurements presented in Fig. 9. The average value is 0.547, as expected (see above). For pure Stokes V the expected value of 0.406 is found.

Magnified by the large number of charge transfers during demodulation, any effect due to transfer loss increases with integration time, diluting the polarization signal. The effect can be used to determine the transfer inefficiency ϵ if one knows how it is related to the degradation of the polarization signal. The ZIMPOL II 4-fold demodulation scheme is rather complicated. Each shifting cycle consists of 10 steps: 6 shifts and 4 accumulation periods. It is not possible to derive a simple analytical formula in closed form that gives the degradation as a function of ϵ and the number of shifting cycles. The degradation can, however, be calculated with an iterative model, which takes into account charge transfer losses to second order. Degradation curves for the linear polarization signal, which are obtained by iterating the calculation up to 500 000 cycles (10 sec integration time for 50 kHz modulation) for different transfer losses, are presented in Fig. 7. The measured degradation is marked by crosses. From the figure ϵ can be estimated to be $(1.5\pm0.3)\times10^{-8}$. This value is about a factor of 200 smaller (better!) than the value specified by the CCD manufacturer, probably due to different definitions of the charge transfer inefficiency. Here ϵ characterizes the relative charge loss for one single transfer. The specifications of the manufacturer seem to give the *charge inefficiency product* (Beynon 1977), which is defined as ϵn, where n is the number of vertical shifts needed to read-out a frame, i.e., the number of rows.

3. Calibration of the polarimeter

In our polarimetry system polarization information is converted into time-dependent intensity information by the modulator. The intensity function is decoded by a CCD, which is used as a synchronous demodulator. To extract the polarization information one has to know the relations between the physical polarization signal and the processed digital data. These relations are found through a calibration procedure that has to account for various types of instrumental effects that can occur in different parts of the system:

- In the modulator package: Wrong retardation amplitude and orientation angle of the modulator induces crosstalk from I to Q.
- In the microlenses: Scattered photons modify the charge distribution and simulate a false polarization signal.
- In the CCD: Polarization gain table effects are caused by the varying charge transfer efficiency. Dark-current produces an offset.
- In the synchronisation of modulation and demodulation: False phase angle.
- In the shifting scheme: Unequal length of the integration phases.

Calibration of the modulation amplitude

Expanding the modulation function for Stokes Q in terms of Bessel functions we find that light with an amount Q/I of linear polarization becomes modulated according to

$$I(t) = \frac{1}{2}[I + J_0(A)Q] + Q\sum_{n=1}^{\infty} J_{2n}(A)\cos(2n\omega t).$$

After demodulation the measured normalized signal $C_{\rm lin}$ is proportional to

$$\frac{Q}{I + J_0(A)Q},$$

which is proportional to Q/I only if $J_0(A)$ vanishes. A deviation of the retardation amplitude A from the value 2.405 (first zero of J_0) leads to Stokes I-like structures in the fractional polarization image. For this reason A should be set to 2.405 radians. This is done by making calibration measurements with an input of 100 % Stokes Q for different values of A, tuning A until no Stokes I-like features remain in the polarization image. This is, however, only possible for the center region of the PEM (for the test measurements we did not correct for any final mismatch; the method used to correct for the sinusoidal retardation distribution is described in Bernasconi 1997.).

Correction for stray light in the microlenses
A small number of photons is scattered at the electrode structure of the CCD surface and contaminates the charge distribution in the pixel rows. Asymmetric contaminations, which for example arise from microlens imperfections in combination with slightly off-axis illumination, can when calculating $C_{\rm circ}$ produce a signal that is the derivative of the spectrum with respect to wavelength. Therefore, spurious Stokes V-like features in the absorption lines may appear. As the scattering coefficients are different for each pixel quadruplet, the correction is separately done for all charge packages. The scattering coefficients are measured for each distinct illumination of the CCD (thus for each setting of the spectrograph), because they are determined by the structure of the sensor as well as by the geometry of the incoming light. The measurement is done without demodulation, i.e. without shifting the charges to and fro on the CCD.

Calibration of the phase angle
The demodulation is synchronized with the reference signal from the piezoelastic modulator driver, which is delayed by a phase shifter (see Fig. 1). The phase between modulator and demodulator is adjusted for maximum Stokes Q signal, which is more sensitive to the phase angle than the Stokes V signal (see Fig. 5).

Nonlinearity
The influence of a small non-linearity coupled with instrumental polarization and /or bias errors on the polarimetric accuracy has been discussed by Keller (1996), who concludes that, for polarization signals larger than 10^{-4}, the influence of a small non-linearity can be neglected. The deviation from linearity was measured to be less than 1 % over the whole sensitivity range of the CCD. The nature of this - for our purposes negligeable - effect is not yet understood.

Unequal lengths of the integration time phases
An unequal length of the demodulation time windows leads to an unequal charge distribution in the four pixels of each quadruplet, even if unmodulated light is used. Thus, a pseudo-polarization signal is measured even for unpolarized light, leading to an offset in the fractional polarization images. This 'zero-polarization' can easily be calibrated under the same observing conditions (same geometry and integration time), but with the modulator turned off to make the system blind to any real polarization.

Data reduction scheme
For the data reduction the following measurements are required:

- dark current without demodulation (*dc-nodem*)
- exposure without demodulation ($nodem$)
- dark current with demodulation and with the same integration time as used during the observation ($dark - current$)
- real physical measurement ($signal$)
- polarization gain table for Stokes Q/I (*efficiency-Q/I*)
- polarization gain table for Stokes V/I (*efficiency-V/I*)
- 'zero polarization' (*no-modulation*)

A scheme of the complete data reduction procedure is presented in Fig. 8. After averaging each measurement over the total number of exposures (frames) dark current is subtracted. Then the scattering coefficients for each quadruplet are determined from the $nodem$ measurement. After correction for dark-current, the $signal$ measurement, *efficiency-Q/I*, *efficiency-V/I* and *no-modulation* are split into four subarrays 1, 2, 3, and 4, corresponding to the four charge packages q_1 to q_4. Each row is corrected for the stray light contributions of the adjacent lines according to the shifting scheme and the measured scattering coefficients. The corrected subarrays are combined according to the definitions of the normalized differences $C_{\rm lin}$ and $C_{\rm circ}$. The zero-polarizations *Zerop Q/I* and *Zerop V/I* are subtracted from the signal and the corresponding efficiency measurements. A 5 pixel median filter eliminates blind quadrupels (pixels with very low quantum efficiency) and charge-traps (pixel-pairs with very low and asymmetric charge transfer efficiency). The signals are finally corrected for the efficiency and clipped to eliminate the disturbing influences of the median filter at the edges of the array.

4. Test observations

The new 2-D polarimeter was tested at two solar telescopes between March and July 1996. For the first time Stokes I, Q/I, and V/I were measured simultaneously with a single CCD. The small polarization signals from the Sun were used to characterize the sensitivity of the polarimeter system and to investigate problems that arise when dealing with signals on the order of 10^{-3} of the intensity and below.

At the *Zürich Solar Tower* the calibration procedure and data reduction scheme were tested. Linear polarization due to resonant scattering near the solar limb was measured with an accuracy of 10^{-4}. The noise level was 10^{-3} in a single frame. By frame averaging the noise level could be reduced to 2×10^{-5}. Spectropolarimetric measurements in a sunspot demonstrated the sensitivity of the instrument to circular polarization. Stokes I, Q/I, and V/I were recorded simultaneously in a sunspot in the lines Fe I 5250 Å and 6302 Å, and in Na I D_2 5890 Å. The Stokes V measurements initially showed artificial parasitic Stokes V signals on the order of 10^{-3}, a problem caused by stray light in the microlenses. This problem could be overcome

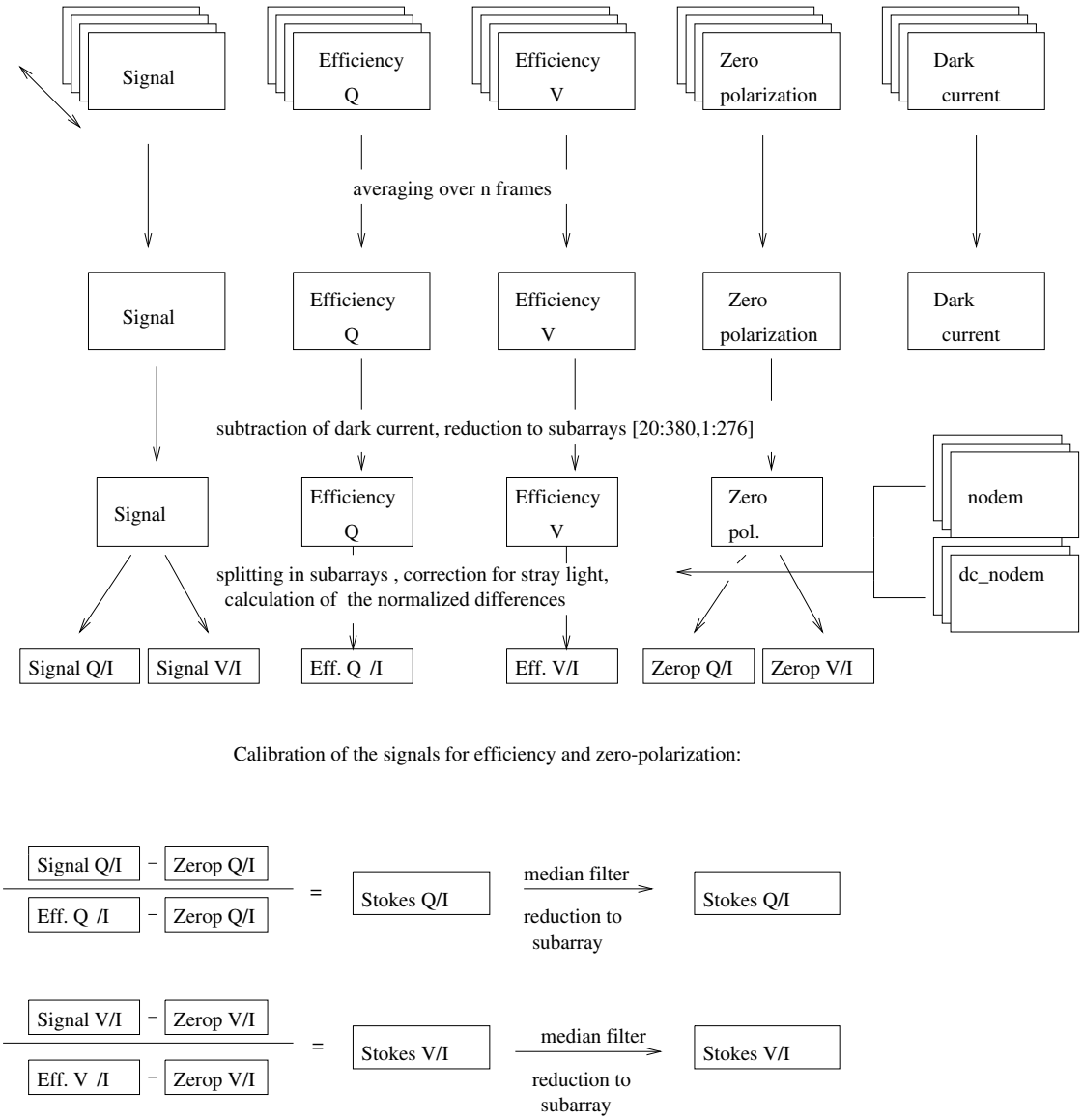

Fig. 8. Scheme of the data-reduction procedure. Explainations are given in the text.

by a more sophisticated data reduction procedure that takes the stray-light contributions into account.

The advanced data reduction scheme was tested during an observing run at the Vacuum Gregory-Coudé telescope of IRSOL (*Istituto Ricerche Solari Locarno*) and its high resolution spectrograph in July 1996. To demonstrate the sensitivity to Stokes V, Zeeman polarization in an active region was recorded in the iron line at 6302.5 Å. The integration time was 1 s per frame, with 50 frames averaged. The Fe I line is accompanied by two telluric lines of O_2, which can be used as indicators of instrumental artefacts: These lines must be invisible in the fractional polarization images. The recorded spectra are presented in Fig. 9. The Stokes I, Q/I and V/I images cover 46 arcsec by 1.3 Å. The Stokes Q/I and Stokes V/I spectra correspond to the polarization images at position of 21 arcsec (one single line). The noise (10^{-4}) is compatible with the expected photon noise. At that level, no artificial polarization features are visible in the two telluric lines at 6302.0 Å and 6302.76 Å. Polarimetry provides the possibility to investigate spectral features that cannot be detected in the normal intensity spectrum, but are visible in the Stokes Q spectrum. The Stokes Q/I spectrum observed near the solar limb has been refered to as *the second solar spectrum* (Stenflo and Keller 1996). It is formed by scattered photons. As an example the hyperfine structure of the Ba II line at 4554 Å is shown in Fig. 10. The measurements were carried out with the Vacuum Gregory-Coudé telescope of IRSOL and its high resolution spectrograph. The entrance slit of the spectrograph was oriented parallel to the solar limb and exposures were taken at different heliocentric angles to investigate the center-to-limb variation of the polarization in the different hyperfine components of the spectral line. The upper part of Fig. 10 illustrates the intensity spectrum around 4554 Å with the Ba II line and an

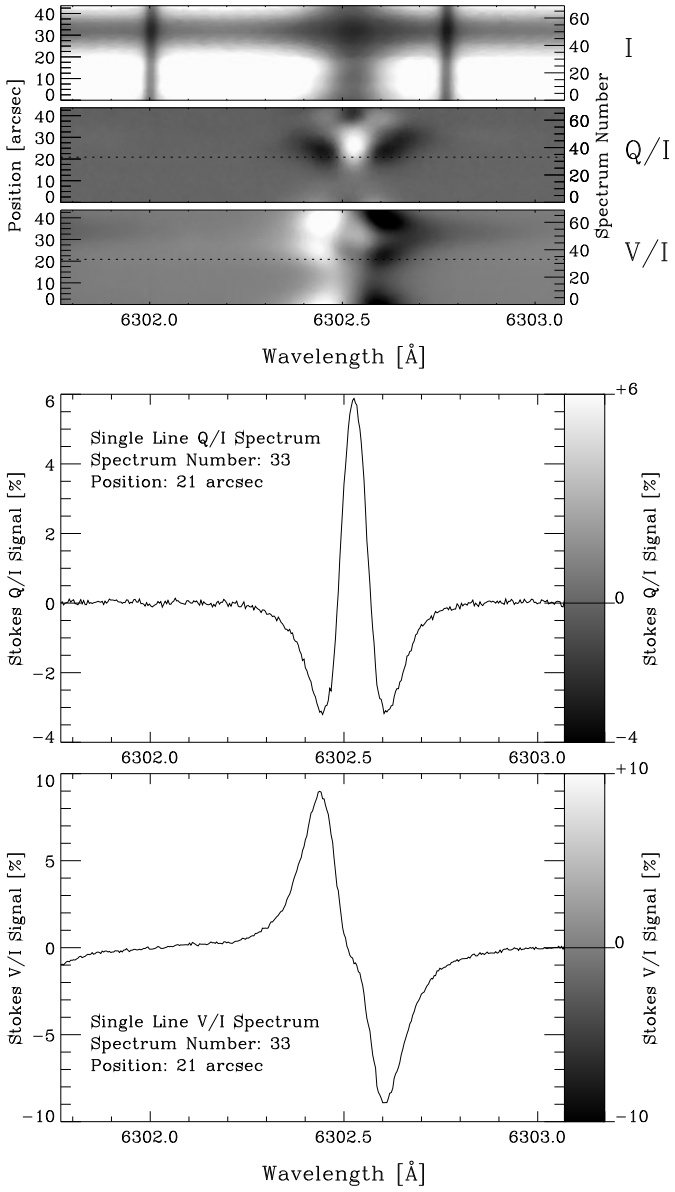

Fig. 9. Zeeman polarization of Fe I in a sunspot recorded at IRSOL in July 1996. Stokes $I, Q/I, V/I$ have been recorded simultaneously. The spectra correspond to polarization images at position of 21 arcsec as indicated by the dotted line. The data have been averaged over 50 frames with 1 s integration time each. No Fourier filter or any other noise reduction technique has been applied. The gray-scales of the Q/I and V/I images are shown in the lower figure.

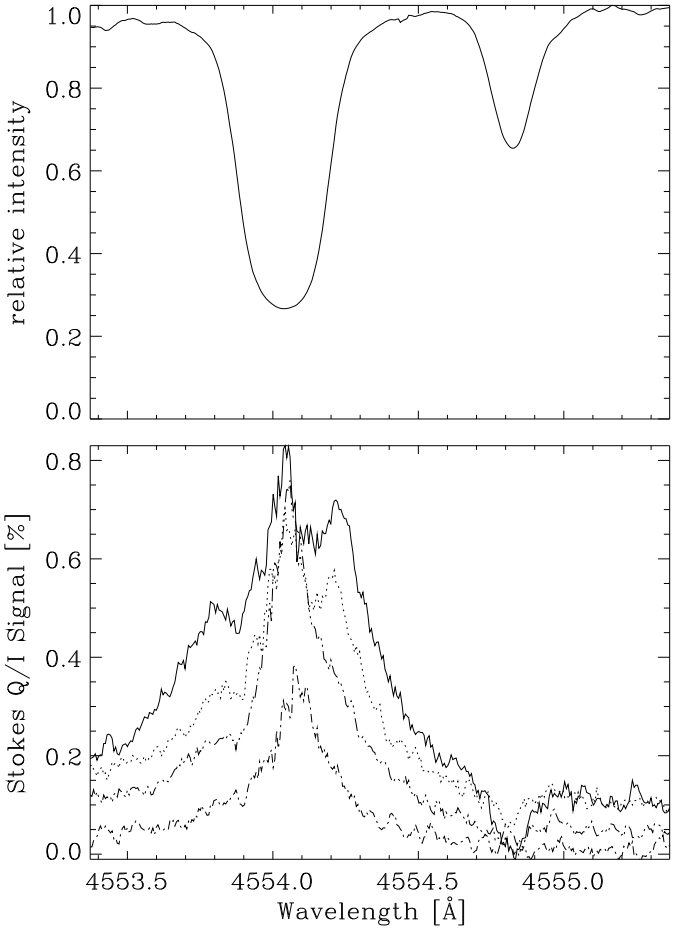

Fig. 10. Stokes I spectrum around 4554 Å with the Ba II line at 4554.0351 Å and the Cr I line at 4554.8229 Å and Stokes Q/I spectra for different distances from the solar limb. The polarization decreases with increasing heliocentric angles θ, ranging from μ =0.05, μ =0.1, μ =0.15,μ =0.2, μ being cos θ.

adjacent line of Cr I, while the lower part shows the decrease of the polarization signal of the Ba II line with increasing heliocentric angles θ, at μ = 0.05, μ = 0.1, μ = 0.15 and μ = 0.2, μ being cos θ. Even with the high spectral resolution of the VGC spectrograph, it is not possible to resolve the hyperfine structure in the intensity profile of the Ba II line, because of Doppler and pressure broadening and line saturation. The polarized Q/I components are narrower, have different intrinsic polarizabilities, and are clearly separated. The central peak, which is due to the even isotopes, is accompanied by a doublet structure of the odd isotopes with nuclear spin $3/2$. More information on this line and its second solar spectrum can be found in Stenflo and Keller (1996) and Stenflo (1997a,b). The presented spectra have been averaged along the spatial (column) direction (average of 69 individual spectra on the CCD) and averaged over 100 exposures of 8 s each.

5. Conclusions

It has been demonstrated that our 2-D polarimeter can be used for precision polarimetry as needed for detailed quantitative research on solar magnetic fields. The principle of using three out of four pixel rows for temporary buffer storage was shown to be feasible. The polarimetric accuracy in the first test measurements is better than 10^{-4}. A noise level of 10^{-3} in a single exposure is achieved. By frame averaging and averaging over the columns, which are oriented parallel to the spatial direction, the noise level could be reduced to 2×10^{-5}, corresponding

to the expected photon noise. The measured efficiency of the modulation-demodulation system shows no deviation from the calculated theoretical performance. The average polarimetric efficiency for the entire polarimeter for linearly polarized light is, after correction for stray light and zero polarization, 54.7 %, in agreement with the calculated value. For circularly polarized light 40.6 % was found, as expected. The values for the individual pixel quadruplets vary due to intrinsic effects, such as asymmetric charge transfer inefficiency or inhomogenities of the microlenses. The last point is of great importance. The high ratio between the focal length of 1 mm and the tolerated lateral focus deviation on the CCD surface of a few μm requires a precise alignment of the camera with respect to the optical axis. The stray light contribution in the masked rows depends critically on the geometry of the illumination. This makes it necessary to calibrate for stray light at exactly the same spectrograph setting as used for the measurement. To avoid calibration errors due to a change of the illumination geometry, all calibration measurements have to be repeated several times during the observations. Spectral features (intensity gradients) in combination with imperfections of the microlenses, a rotation of the microlens array with respect to the CCD, and slightly off-axis illumination lead to a variation of the stray-light content from one pixel quadruplet to the other. The polarimeter is calibrated for each individual pixel quadruplet. It was pointed out that the calibration of each quadruplet not only depends on intrinsic sensor properties, but also on the illumination.

We consider three improvements to the polarimeter described in this paper:

- To use a chip that has been coated by the manufacturer with an opaque mask during the fabrication process. Then only the microlens-array has to be aligned relative to the mask, which is less critical than mounting and aligning a microlens-mask assembly.
- Separation of two adjacent quadruplets by an additional buffer row. This fifth row separates row 1 of the second quadruplet from row 4 of the first quadruplet. Thus stray light from the adjacent pixel quadruplet $i + 1$ is collected in the buffer row and cannot contaminate quadruplet i. This requires a mask with 5 rows per period, one unmasked and four covered by an opaque mask. The microlens aperture must be 5 rows wide. The only disadvantage is the 25% loss of spatial resolution, due to the 25% larger image element.
- For observations with low spectral resolution at telescopes with a small focal ratio, which provides a high photon flux, a masked detector without microlenses could be used. As a factor of four in photon efficiency is lost, such a system is useful only for observations where long integration times can be tolerated.

We have demonstrated here that, despite the problems encountered in using this new type of polarimeter, high polarimetric accuracy can be achieved by careful calibration. This is a very encouraging result and a great motivation to further improve the system.

Acknowledgements. We are grateful to U. Egger for developing and constructing parts of the electronics of the polarimeter, P. Steiner for developing the software to control it, and F. Aebersold for constructing the mechanical parts. We also thank J.O. Stenflo, C.U. Keller, F.-L. Deubner and P.N. Bernasconi for interesting discussions on topics concerning this paper. We are very thankful to M. Bianda for providing observing time at IRSOL at Locarno and to J. Tinbergen for carefully reading and commenting on the manuscript. This work was partly supported by the Swiss National Science Foundation, grant No. 2000-043048.95/1, which is gratefully acknowledged.

References

Bernasconi P.N., 1997, Ph.D. Thesis, No.12227, ETH, Zürich, p.27, in press

Bernasconi P.N., Keller C.U., Solanki S.K., Stenflo J.O., 1997, A&A, in press

Beynon J.D., Lamb D.R., 1977, Charge-Coupled Devices and their Applications. Mc Graw-Hill Book Company, London

Collet E., 1993, Polarized Light - Fundamentals and Applications. Marcel Dekker, Inc., New York/Basel/Hong Kong.

Gale M.T., Pedersen J., Schütz H., Povel H.P., Gandorfer A.M., Steiner P., Bernasconi P.N., 1997, Optical Engineering Vol.36, No.5, 1510

Keller C.U., 1996, Solar Phys. 164, 243

Keller C.U., Aebersold F., Egger U., Povel H.P., Steiner P., Stenflo J.O., 1992, LEST Foundation Technical Report No. 53. Institute of Theoretical Astrophysics, University of Oslo

Keller C.U., Deubner F.-L., Egger U., Fleck B., Povel H.P., 1994, A&A 286, 626

Kemp J.C., 1969, Journal of the Optical Society of America 59, 950

Povel H.P., 1995, Optical Engineering 34, 1870

Povel H.P., Aebersold H., Stenflo J.O., 1990, Appl. Opt. 29, 1186

Povel H.P., Keller C.U., Yadigaroglu I.-A., 1994, Appl. Opt. 33, 4254

Rüedi I., Keller C.U., Solanki S.K., 1996, Solar Phys. 164, 265

Stenflo J.O., 1982, Solar Phys. 80, 209

Stenflo J.O., 1994, Solar Magnetic Fields - Polarized Radiaton Diagnostics. Kluwer, Dordrecht, p.73

Stenflo J.O., 1997a, A&A, in press

Stenflo J.O., 1997b, in N. Mein (ed.), Forum Themis, Proc. Conf. at Meudon, 14-15 Nov. 1996, p. 219

Stenflo J.O., Keller C.U., 1996, Nat 382, 588

Stenflo J.O., Keller C.U., Povel H.P., 1992, LEST Foundation Technical Report No. 54. Institute of Theoretical Astrophysics, University of Oslo

Stockman H.S., 1982, Instrumentation in Astronomy IV, Proc. SPIE 331, 76

This article was processed by the author using Springer-Verlag LaTeX A&A style file *L-AA* version 3.